Cell Adhesion-Dependent Biphasic Axon Outgrowth Elucidated by Femtosecond Laser Impulse

Sohei Yamada[a,b,†,*], Kentarou Baba[c,†], Naoyuki Inagaki[c], Yoichiroh Hosokawa[a,d,*]

[a] Division of Materials Science, Nara Institute of Science and Technology, 8916-5 Takayama, Ikoma, Nara 630-0192, Japan

[b] Graduate School of Science and Technology, Hirosaki University, 3 Bunkyo-Cho, Hirosaki, Aomori, 036-8561, Japan

[c] Division of Biological Science, Nara Institute of Science and Technology, 8916-5 Takayama, Ikoma, Nara 630-0192, Japan

[d] Medilux Research Center, Nara Institute of Science and Technology, 8916-5 Takayama, Ikoma, Nara 630-0192, Japan

[†] These authors contributed equally

*Corresponding authors: Sohei Yamada, so-yamada@hirosaki-u.ac.jp and Yoichiroh Hosokawa, hosokawa@ms.naist.jp

Abstract

Axon outgrowth is promoted by the mechanical coupling between F-actin and adhesive substrates via clutch and adhesion molecules in an axonal growth cone. In this study, we utilized a femtosecond laser-induced impulse to break the coupling between the growth cone and the substrate, enabling us to evaluate the strength of the binding between the growth cone and a laminin on the substrate, and also determine the contribution of adhesion strength to neurite outgrowth and traction force for the outgrowth. We found that the adhesion strength of axonal L1 cell adhesion molecule (L1CAM)-laminin binding increased with the laminin density on the substrate. In addition, fluorescent speckle microscopy revealed that the retrograde flow of F-actin in the growth cone was dependent on the laminin density such that the flow speed reduced with increasing L1CAM-laminin binding. However, neurite outgrowth and the traction force did not increase monotonically with increased L1CAM-laminin binding but rather exhibited biphasic behavior, in which the outgrowth was suppressed by excessive L1CAM-laminin binding. Our quantitative evaluations suggest that the biphasic outgrowth is regulated by the balance between traction force and adhesion strength. These results imply that adhesion modulation is key to the regulation of neurite outgrowth.

Introduction

During neuronal development, axons elongate and form functional connections with other neurons and relevant cells. The axonal migration is an essential process to regulate formation and regeneration of neuronal network. The previous studies proposed that extracellular guidance cue (chemical ligands) induces the axon outgrowth[1,2]. The growth cone located at the tip of an elongating axon senses chemical ligands in the external environment and undergoes directional migration[1-3]. In addition, growth cone senses a rich source of the extracellular matrix (ECM) to facilitate directional migration. An adhesion coupling between the growth cone and its substrate induces rapid migration and axon outgrowth.

The traction force underlying growth cone migration is regulated by modulation of the coupling efficiency between actin filament (F-actin) retrograde flow and adhesive substrates via clutch and cell adhesion molecules[4,5]. Thus, the traction force transmitted to the substrate through the F-actin-adhesion coupling promotes axon outgrowth[1,6].

We previously identified shootin1a and cortactin as clutch molecules for growth cone migration[7,8]. These molecules mediate the linkage between F-actin retrograde flow and the cytoplasmic domain of L1 cell adhesion molecule (L1CAM)[9]. The extracellular domain of L1CAM interacts with adhesive ligands such as laminins in the extracellular matrix[10-12]. L1CAM linked to the F-actin flow undergoes gripping (stop) and slipping (retrograde flow) on the substrate. It is the balance between these grip and slip states that regulates growth cone migration[12].

Our investigation focuses on the mechanism by which the interaction between L1CAM and laminin generates force. The challenge is to quantify key processes of growth cone migration, for which the adhesion strength via L1CAM-laminin binding is fundamental. However, it is difficult to quantify adhesion strength by conventional methods. For instance, the shear flow assay[13,14] is not suitable for evaluating local adhesion at the interface between a growth cone and the substrate, whereas it is difficult to apply single-cell force spectroscopy[15,16] to evaluate force without disturbing the adhesion required for axon outgrowth. The adhesion strength of migrating growth cone was previously evaluated form a detachment by micromanipulation with calibrated glass needles[17]. However, these methods are not suitable for the evaluation of adhesion strength at the growth cone level. Therefore, the relationship between adhesion strength and axon outgrowth has not been comprehensively elucidated. We thus developed a method utilizing a femtosecond laser-induced impulsive force, which we used to quantify adhesions between leukocytes and endothelial cells, among epithelial cells, and between neurons and mast cells[18,19].

A near-infrared femtosecond laser focused through an objective lens into a water solution generates stress and shock waves at the laser focal point. Vogel and his co-workers have observed these generation processes and the propagation dynamics, and confirmed that the femtosecond laser pulse generates stress waves with the smallest photon energy and confines the propagation

in the smallest area compared to other pulsed lasers[20,21]. Referring the experimental results, we construct a simplified model to explain the action of these waves to small particles near the laser focal point and confirmed the reliability with experiments. Based on these results, the action is approximated that these waves propagate out spherically and act as an impulsive force on nearby cells. As the force is localized to a diameter of 1–10 μm and breaks intercellular adhesions at a single-cell resolution, we considered the impulse could be used to assess adhesion of the growth cone.

We also developed an original method to quantify the magnitude of the impulsive force by using atomic force microscopy (AFM)[22], enabling us to quantify the strength of intercellular adhesions on the basis of the force needed to break the connection[18,19,23]. In this method, the force is estimated from vibration of the AFM cantilever which placed instead of the cell samples. The vibration was analyzed with taking propagations of shock and stress waves into account, and then the total force generated at the laser focal point was estimated as a function of the laser pulse energy. We can calibrate the force to break adhesion of the growth cone by applying this estimation to the geometrical relation between the laser focal point and the growth cone to break the adhesion.

In this work, we applied our previously established methods for generating laser-induced impulsive force[7,12] to investigate the contribution of L1CAM-laminin binding to axon outgrowth. The specific interaction between laminin and L1CAM was confirmed by L1CAM knockdown in neurons. The strength of L1CAM-mediated adhesion was confirmed to be dependent on the density of laminin on the substrate. In addition, we used fluorescent speckle microscopy to observe the motions of F-actin and L1CAM in the axonal growth cone and then further assessed the contribution of L1CAM-laminin binding to F-actin-substrate coupling. These results were compared with axon outgrowth and traction force for the outgrowth as a dependence of laminin density on the substrate. We propose a mechanism of neurite outgrowth that depends on the density of laminin on the substrate, identifying L1CAM–laminin binding as a key regulator of this process.

Results

Adhesion breaking by a femtosecond laser-induced impulsive force

Hippocampal neurons cultured for 3 days on a glass-bottom dish coated with 10 μg/ml laminin were placed on an inverted microscope equipped with a femtosecond laser irradiation system. The single-shot femtosecond laser pulses were focused in the vicinity of axonal growth cones to assess the adhesion breaking threshold (Fig. 1A). The force was estimated by measuring the distance from the growth cone at which the laser pulse broke the adhesion to the substrate. For example, the laser with a pulse energy of 700 nJ was initially focused at a position 20 μm from a targeted growth cone. After the first pulse irradiation, the focal point was moved closer to the target

107 in 5 μm steps via an electrical microscope stage until adhesion was broken; the distance between
108 the growth cone and the final laser focal position was recorded.
109 Representative result of the adhesion breaking of the growth cone is shown in Fig. 1B and
110 Video S1. The growth cone moves on μm scale in the differential interference contrast (DIC) images
111 before and after the laser irradiation at the final laser focal point. Such displacement was only
112 observed at the final laser irradiation point. The distance between the growth cone and the final
113 point became greater with increasing the pulse energy (Fig. 2A). The detachment of the growth
114 cone due to force loading may result from the dissociation of laminin from the substrate. To confirm
115 this possibility, fluorescent dye-conjugated laminins were coated onto the grass-bottom dish, and
116 their fluorescent intensity was monitored following impulsive force loading. As shown in Fig. S1, no
117 significant change in fluorescence intensity was observed around laser focal point. In addition, we
118 have confirmed that the effects of cavitation and temperature are negligible for the cell detachment
119 by the femtosecond laser impulse. These findings suggest that the axonal detachment results from
120 the dissociation of L1 from laminin rather than the detachment of laminin from the substrate. This
121 observation indicates that growth cones can be selectively detached from the substrate by the
122 laser-induced impulsive force.
123
124 ***Quantification of the adhesion breaking force***
125 We evaluated the threshold distance (*R*) to break growth cone adhesion to the glass
126 surface coated with 10 μg/ml laminin at different laser pulse energies (*L*) (Fig. 2A). As the impulsive
127 force near the growth cone increases with *L*, the positive correlation between *R* and *L* indicates
128 that *R* increases with an increasing impulsive force. We quantified the threshold for breaking the
129 adhesion by using our previously established AFM method[24] in which an AFM cantilever replaces
130 the tip of the growth cone and the impulsive force loaded on the cantilever is estimated from its
131 bending movement[18] as a function of *L*. From the estimation, the impulsive force F_0 generated at
132 the laser focal point is related to *L* as follows:
133 $F_0 = -0.003573L^2 + 0.644L - 1.5758.$ [1]
134 Because the water medium absorbs the pulse with nonlinear processes such as multi-
135 photon and multi-cyclic absorption, the force increases nonlinearly with the pulse energy.
136 Therefore, although the curve in Fig. 2A looks linear in energy, it does not mean that the impulsive
137 force F_0 increases linearly with *R*. Assuming that F_0 propagates spherically in the vicinity of the
138 laser focal point, the impulsive force as a unit of pressure (*P*) is expressed by the following equation:
139 $P\ (\mathrm{kPa}) = \frac{F_0\ (\mu\mathrm{N}) \times 10^3}{4\ \pi R^2\ (\mu m^2)}.$ [2]
140 Fig. 2B is a plot of pressure to break the growth cone adhesion calculated with Eq. [2] for
141 each data point in Fig. 2A. The mean value of the minimum pressure to break growth cone adhesion

142 to a 10 μg/ml laminin substrate was 4.35 ± 1.08 kPa, comparable with the breaking threshold
143 reported in our previous study[23,24].
144
145 ***Adhesion strength of the growth cone depends on L1CAM-laminin binding***
146 Fluorescent dye-conjugated laminin was used to assess the density of laminin on the glass
147 substrate. The bright spots in images in Fig. 2C are aggregates of laminin less than 1 μm in size.
148 The number of aggregates increased with concentration (*C*) of laminin used to coat the glass and
149 saturated when *C* > 50 μg/ml. The fluorescence was observed not only from the aggregates but
150 also from the substrate. The intensity of fluorescence (*I*) increased with *C* until reaching saturation
151 (Fig. 2D). This result implies that the number of laminin molecules attached to substrate *N* is not
152 proportional to *C* but saturates when *C* > 50 μg/ml. Here we use *I* as an index of coverage of
153 laminin on the substrate. The saturation of *I* is simply expressed by an exponential plateau curve:
154 $I = I_{max}\left(1 - e^{-C/k}\right)$ [3]
155 We assumed that (i) *I* is proportional to the number of laminin molecules attached to
156 substrate *N*; (ii) *N* has a maximum that determines I_{max}. The constant *k* presumably reflects
157 attachment of laminin molecules on the substrate, which are induced by collision of the laminin
158 molecules to the substrate on the coating period (12 h in this experiment). In addition, we neglected
159 the dissociation of laminin from the substrate because *I* was not significantly different after replacing
160 the medium to one without laminin for the laser irradiation experiment. We defined the coverage
161 (*A*) of laminin as an index of laminin density on the substrate using the following equation:
162 $A = 1 - e^{-C/k}$ [4]
163 An *A* of 1 means that the laminin attached maximumly on the substrate. The constant *k*
164 was estimated by least-squares fitting with Eq. [3] from the data in Fig. 2D to obtain *A* on the
165 substrate coated with laminin solution at concentration *C*.
166 The breaking threshold was evaluated according to *A* (left plots in Fig. 3A) and compared
167 with that determined at L1CAM-knockdown samples (right plots in Fig. 3A). The threshold with
168 respect to the coverage of laminin increased with *A* (Fig. 3B). On the other hand, the L1CAM-
169 knockdown samples maintained thresholds that matched those shown by controls at the low
170 coverage (*A* = 0.01). As the expression of L1CAM is almost suppressed by RNAi[12] (see also
171 Materials and Methods), the major adhesion of the control sample is not due to L1CAM-laminin
172 binding. These findings indicate that the adhesion strength between the growth cone and substrate
173 is strengthened by L1CAM-laminin binding. The offset threshold (~2.5 kPa) likely reflects laminin-
174 independent adhesive interactions.
175 The increase in adhesion strength with increasing *A* in the control samples (Fig. 3B)
176 suggests that the adhesion strength due to the L1CAM-laminin binding increases with the laminin
177 density on the substrate, despite the variability as a result of individual differences among the cells.

178 As the adhesion strength is integral to the individual binding strength between L1CAM and laminin,
179 the adhesion strength reflects the number of L1CAM-laminin interactions. Thus, the increase in the
180 breaking threshold with *A* may reflect the increase in the number of the L1CAM-laminin interactions
181 that occur with increased laminin density. This relationship is presumably satisfied until the L1CAM
182 sites available for binding are saturated.
183
184 ***L1CAM-laminin binding promotes F-actin-adhesion coupling***
185 The contribution of the laminin coverage *A* to F-actin-adhesion coupling in the retrograde
186 flow was investigated next by visualizing F-actin and L1CAM molecules in filopodia at the growth
187 cone. F-actin dynamics were observed by the motion of fluorescent actin speckles tagged with
188 HaloTag (Fig. 4A; Video S2; Video S3; Video S4) which were observed moving along filaments
189 toward the leading edge of the growth cone. The speed at which they moved decreased linearly
190 with increasing *A*, slowing from 3.70 μm/min at an *A* of 0.06 to 2.29 μm/min at an *A* of 0.99 (Fig.
191 4B). These data suggest that *A* promotes the cytoskeletal-adhesion coupling.
192 The dynamics of L1CAM-laminin binding were evaluated as grip and slip motions of
193 L1CAM-HaloTag as shown in Fig. 4C (Video S5; Video S; Video S7). The ratios of grip and slip
194 states increased and decreased, respectively, with increasing *A* (Fig. 4D). Consistent with this, the
195 speed at which HaloTag traveled (i.e., flow speed) decreased (Fig. 4E) while the duration spent in
196 the grip phase increased (Fig. 4F) with increasing *A*. The differences between slip and grip states
197 were proportionate to *A* in the range of 0.06 to 0.99.
198 L1CAM-laminin binding promotes the L1CAM grip state, transmitting the traction force to
199 the substrate[12]. With increased cytoskeletal-adhesion coupling, F-actin flow slows and the traction
200 force transmitted to the substrate for growth cone migration increases[4,25]. Therefore, the
201 associations described above support the result from the adhesion breaking test, i.e., the number
202 of the L1CAM-laminin interactions, reflective of the adhesion strength of the growth cone, are nearly
203 proportional to *A*. Conversely, the dissociation of L1CAM-laminin interactions disrupts cytoskeletal-
204 adhesion coupling such that the force of retrograde flow is no longer transmitted to the substrate[12].
205 The grip and slip motions observed in this study indicate that L1CAM-laminin binding is not static
206 but changes dynamically. Thus, when the average number of L1CAM-laminin interactions between
207 the growth cone and substrate is increased, the grip state is prolonged.
208
209 ***L1CAM-laminin binding results in biphasic axonal migration***
210 To examine the effect of laminin coverage on growth cone migration, hippocampal neurons
211 were transfected with either control RNA or L1CAM miRNA, and their migration was monitored over
212 a 7 h in different concentrations of *A* (Fig. 5A left panels; Video S8). The migration speed of the
213 growth cone did not increase linearly but instead exhibited a biphasic response dependent on *A*:

214 within the range of 0.06 to 0.45, the migration speed exhibited a significantly increased, whereas
215 within the range of 0.45 to 0.99, it was markedly reduced (Fig. 5B). In neurons with L1CAM RNAi,
216 the migration speed significantly decreased compared to Control RNAi. Notably, the biphasic
217 migration pattern of the growth cone was abolished in the L1CAM knockdown neurons (Fig. 5A,
218 right panels; Video S8).
219
220 ***L1CAM-laminin binding results in biphasic axon outgrowth***
221 Axon outgrowth also depends on the laminin coverage (*A*), as shown in Fig. 6. Axon lengths
222 were the longest (>130 μm) when neurons were cultured under conditions where *A* was between
223 0.78 and 0.95. However, the lengths of axons from L1CAM knockdown neurons were not affected
224 by *A* (blue box in Fig. 5B), with shorter axons overall. These data suggest that axon outgrowth is
225 regulated by the L1CAM-laminin binding to the laminin substrate and that the regulation is biphasic.
226
227 ***Traction force for the axon outgrowth exhibits biphasic behavior***
228 Traction force microscopy was utilized for monitoring the force loaded on the substrate in
229 the axon outgrowth. In this method, the traction force is observed as displacement of the fluoresce
230 microbeads enclosed in the substrate and quantified from the bead shift from original position to
231 displaced position in the axon outgrowth (Fig. 7A). At the region of the growth cone, the mean force
232 for A = 0.45 (35 pN/nm^2) was larger than not only that for A = 0.01 (25 pN/nm^2) but also that for A
233 = 0.99 (25 pN/nm^2) (Fig. 7B). The dependence, which is not monophasic but biphasic, is similar to
234 that for axon outgrowth (Fig. 5), suggesting that the traction force is directly related with the axon
235 outgrowth.
236
237 **Discussion**
238 In this study, we quantified adhesion strength of axonal growth cone (Fig. 3B), axon
239 elongation (Fig. 5, 6), and traction force of growth cone in the elongation (Fig. 7B) as a function of
240 laminin density on the substrate. In addition, we evaluated molecular dynamics of F-actin and
241 L1CAM in the growth cone (Fig. 4). Although the adhesion strength increased with the laminin
242 density, the laminin dependency of the axon elongation and traction force indicated biphasic
243 behavior. These differences revealed in the measurements allow us to argue the mechanism of
244 axonal outgrowth promoted by the growth cone.
245 The adhesion strength measured by femtosecond laser impulses is not only for the
246 adhesion between L1CAM and laminin but for total amount of the adhesion including other specific
247 and nonspecific adhesions. The adhesion strength estimated as the adhesion breaking force is on
248 the order of kilopascals (3-5 kPa). On the other hand, traction force detects the force to promote
249 axon outgrowth. The force is generated by force transmission of F-actin retrograde flow;

250 transmission is effective when the binding forces of the clutch and adhesion molecules between F-
251 actin and substrate are higher than the traction force[12]. The force is estimated in the range 20 – 50
252 pN/μm^2. Since the unit of force for traction (pN/μm^2) corresponds to pascals (Pa = N/m^2), the
253 adhesion strength is about 100 times larger than the traction force (0.02 – 0.05 kPa). As shown in
254 Fig. S1, the laser impulse does not directly break the laminin on the substrate. This means the
255 adhesion breaking force in Fig. 3 reflects the adhesion between the growth cone and the substrate.
256 The traction force in Fig. 7 is the force transmitted by the F-actin retrograde flow. Conclusively, our
257 results suggest that the adhesion between the growth cone and the substrate is strong enough to
258 transmit the force of F-actin retrograde flow to the substrate.

259 The L1CAM-laminin interactions promote the axon outgrowth transmitting the force of F-
260 actin retrograde flow to the substrate[26]. In this study, we confirmed that axon outgrowth depends
261 on laminin concentration, incorporating adhesion strength and traction force. When the laminin
262 density is low, F-actin is not coupled to the adhesive substrate through clutch molecules (e.g.,
263 shootin1a and cortactin) and L1CAM. As a result, the force of retrograde flow is not effectively
264 transmitted to the substrate to produce sufficient traction for axon outgrowth. This was
265 demonstrated by the short axon lengths of neurons cultured on the substrate with low laminin
266 density. By contrast, the rate of retrograde flow slows as the laminin density increases, indicating
267 greater cytoskeletal-adhesion coupling that promotes transmission of the force from the flow to the
268 traction force for growth cone migration. Our results indicate that laminin densities resulting in an
269 *A* between 0.45 and 0.78 are optimal for providing suitable traction force. Interestingly, we observed
270 a decrease in axon outgrowth at a high laminin density, suggesting that excessive L1CAM-laminin
271 binding suppresses axon outgrowth.

272 Similar biphasic behavior has been reported depending for concentration of guidance
273 molecules[17,27] and integrin-ligand binding[28-30]. Notably, neurite outgrowth exhibits a biphasic
274 dependence on ligand concentration, with intermediate concentrations resulting in maximal neurite
275 outgrowth[31.] Our results consistent with previous studies, reinforcing the validity of our method. By
276 integrating genetic manipulation, we extend mechanical measurement to provide the specific
277 contribution of L1-laminin interactions to adhesion strength. Moreover, our study extends these
278 findings by demonstrating that traction force generation also exhibits a biphasic dependence with
279 laminin concentration. This integration of force measurement and genetical approaches helps fill
280 the gap between classical adhesion studies and contemporary molecular insights into growth cone
281 migration.

282 Cell adhesion strength was also evaluated by shear-stress flow assay and compared with
283 the migration speed. With strong adhesion, the cells spread and extended lamellae, but the cell
284 body did not move. The suppression of migration was attributed to the inability of cells to overcome
285 adhesion to the substrate[30,32-34]. For axons, outgrowth is promoted not only by the traction force at

286 the forward side but also by detachment of the back side. Thus, the decrease in growth we
287 observed may be attributable to a lack of detachment as a result of excessive L1CAM-laminin
288 interactions which does not couple with the retrograde flow. On this assumption, the traction force
289 is also suppressed by the excessive interaction as well as the axon outgrowth.

290 Notably, axon outgrowth was suppressed when *A* increased from 0.78 to 0.99, an
291 estimated proportional increase in adhesion strength of ~20%. This result indicates that the
292 modification of outgrowth is on the order of 10% of the modification in the adhesion strength as a
293 result of the number of L1CAM-laminin interactions. Our data therefore suggest that these
294 interactions are responsible for adhesion to the substrate and thus for the regulation of axon
295 outgrowth This regulation is key for growth cone migration and axon outgrowth through the
296 extracellular matrix in brain, thereby contributing to the formation of network connections with other
297 neurons and relevant cells.

298 This investigation utilized femtosecond laser impulses to quantitatively evaluate the
299 adhesion strength between axonal growth cones and a laminin substrate. The data show relative
300 contribution of the L1CAM-laminin interactions in adhesion of the growth cone i.e., the strength of
301 the interaction increases with the laminin density. Notably, axon outgrowth does not increase
302 monotonically with increased L1CAM-laminin binding but instead exhibits biphasic behavior, in
303 which outgrowth is suppressed in the presence of high amounts of L1CAM-laminin binding. This
304 biphasic outgrowth is regulated by altered adhesion caused by changes in the number of binding
305 interactions on the order of 10%. These results suggest that the balance between the traction force
306 from the cytoskeletal-adhesion coupling and growth cone adhesion is one of the keys to regulating
307 axon outgrowth. Future studies on the biphasic regulation of axon outgrowth should seek to further
308 elucidate the guidance mechanism.
309

310

311 **Materials and Methods**

312

313 ***Preparation of cell culture substrate***

314 For each experiment, a 35 mm glass-bottom dish (Matsunami, Osaka, Japan) was coated
315 with 100 μg/ml poly-lysine (FUJIFILM WAKO Pure Chemical Corporation) at 37°C for 12 h. After
316 washing, the plate was coated with laminin (laminin 1; FUJIFILM WAKO Pure Chemical
317 Corporation) in phosphate-buffered saline (PBS) at 37°C for 12 h. The surfaces were washed three
318 times with PBS. The laminin density on the dish was modified by altering the concentration of the
319 deposited laminin solution (0.01–100 μg/ml). The laminin density was evaluated by coating the dish
320 with laminin conjugated to a fluorescent dye (green fluorescent HiLyte 488; Cytoskeleton), which
321 was observed under a confocal laser scanning microscope (Zeiss LSM710; excitation, 488 nm;
322 emission, 510 nm). The fluorescence intensity was estimated as an area integration (15 × 15 μm)
323 of the substrate fluorescence.

324

325 ***Cell culture***

326 Hippocampal neurons were prepared from embryonic day 18 rats and seeded on glass-
327 bottom dishes. To induce axon outgrowth, neurons were cultured in neurobasal medium (Thermo
328 Fisher Scientific) containing B-27 supplement (Thermo Fisher Scientific) and 1 mM glutamine for 3
329 days. All relevant aspects of the experimental procedures were approved by the Institutional Animal
330 Care and Use Committee of Nara Institute of Science and Technology.

331

332 ***Femtosecond laser irradiation system***

333 The cultures were imaged on an inverted microscope (IX71; Olympus) utilizing
334 femtosecond laser pulses from a regeneratively amplified Ti:Sapphire femtosecond laser (800 ± 5
335 nm, 100 fs, <1 mJ/pulse, 32 Hz) (Solstice Ace; Spectra-Physics). The pulse was focused near the
336 growth cone (Fig. 1A) through a 100× lens objective (UMPlanFl, numerical aperture [NA], 1.25;
337 Olympus). The irradiation was controlled by a mechanical optical shutter (Σ-65GR; Sigma Koki).
338 The laser pulse energy was tuned by a half-wave (λ/2) plate and dual polarizers. A single
339 femtosecond pulse (50–1,000 nJ/pulse) was applied near the growth cone, and adhesion breaking
340 was monitored by a charge-coupled-device (CCD) camera.

341

342 ***Impulsive force measurement system using AFM***

343 AFM was used to quantify the force needed to break the adhesion, as described
344 previously[18]. An AFM cantilever (thickness, 4.0 μm; length, 125 μm; width, 30 μm; force constant,
345 42 N/m; resonance frequency, 330 Hz in air) (TL-NCH-10; Nano World, Neuchatel, Switzerland)

346 was attached to the AFM head (Nano Wizard 4 BioScience; JPK Instruments, Berlin, Germany)
347 and placed in pure water on the microscope stage. The laser pulse was focused 10 μm away from
348 the top of the cantilever. The transient oscillation of the cantilever induced by the laser pulse
349 irradiation was detected by an oscilloscope. The magnitude of the cantilever movement was
350 estimated from the oscillation.
351
352 ***Evaluation of laminin detachment on the substrate by impulsive force loading***
353 The system for the laser irradiation and the condition of fluorescence laminin-coat are the
354 same as described above. The change in fluorescence intensity before and after laser irradiation
355 was analyzed in estimated shock wave generation area.
356
357 ***L1CAM knockdown experiment***
358 L1CAM knockdown neurons were prepared by using a Block-iT Pol II miR RNAi expression
359 kit (Invitrogen). The targeting sequence of L1CAM miRNA and its effectiveness were reported
360 previously[12]. Hippocampal neurons were transfected with the miRNA expression vector and
361 incubated for 20 h. The cells were then collected and cultured on the laminin-coated glass-bottom
362 dishes. In this system, GFP is expressed with the L1CAM miRNA, enabling the growth cones of
363 transfected cells to be visualized and monitored.
364
365 ***Fluorescent speckle microscopy***
366 The retrograde flow of F-actin and slip and grip motions of L1CAM were investigated by
367 fluorescent speckle microscopy. HaloTag-actin and L1CAM-HaloTag were expressed in
368 hippocampal neurons. To introduce HaloTag tetramethylrhodamine (TMR) to L1CAM-HaloTag and
369 HaloTag-actin, hippocampal neurons were incubated with HaloTag TMR ligand (Promega) at a
370 1:1,500 dilution in L15 medium containing B27 supplement and 1 mM glutamine for 1 h at 37°C.
371 The medium was then replaced with fresh L15 medium. The preparation method of HaloTag-actin
372 is specified in the literature[12].
373 HaloTag-actin speckles were observed at 37°C using a fluorescence inverted microscope
374 (Axio Observer A1; Carl Zeiss) equipped with a C-apochromat 63× NA 1.20 lens objective (Carl
375 Zeiss), an illumination laser (561 nm), and an EM-CCD camera (Ixon3; Andor). Fluorescent
376 L1CAM-HaloTag speckles in growth cones were observed using total internal reflection
377 fluorescence (TIRF) on an inverted microscope (IX81; Olympus) equipped with a TIRF lens
378 objective (UAPON 100×OTIRF NA 1.49; Olympus), an illumination laser (488 nm), and a scientific
379 complementary metal-oxide semiconductor (sCMOS) camera (ORCA Flash4.0LT; HAMAMATSU).
380 The flow speed of F-actin and slip speed of L1CAM were analyzed by monitoring the fluorescence
381 signals of the HaloTags at 5 s intervals. L1CAM puncta that were visible for at least 10 s (two

382 intervals) were analyzed; immobile ones were defined as L1CAM in stop (grip) phase, while those
383 that flowed retrogradely were defined as in flow (slip) phase.
384
385 ***Evaluation of growth cone migration by confocal microscopy***
386 In the neuron, EGFP is expressed to track the growth. The growth cone was
387 monitored by the EGEP fluorescence and DIC images. The surface of polyacrylamide gels was
388 coated with laminin using the same procedure as that used to coat glass-bottom dishes (see
389 above). EGFP and DIC signals were observed at 5 min intervals for 7 h using a fluorescence
390 microscope (IX81; Olympus) equipped with an EM-CCD camera (Ixon DU888; Andor), using a
391 20×/0.8 objective lens. Speed of growth cone migration was measured using ImageJ (Fiji version).
392
393 ***Evaluation of axon length by immunofluorescence staining***
394 Axon length was evaluated by immunofluorescence imaging. Neurons were cultured on
395 polyacrylamide gels coated with laminin for 3 days, fixed with 3.7% formaldehyde in PBS overnight
396 at 4°C, treated for 15 min with 0.05% Triton X-100 in PBS at 4°C, and then incubated with 10%
397 fetal bovine serum in PBS overnight at 4°C. The cells were then incubated with anti-GFP antibody
398 (MBL, 598) and anti-Tubulin β3 (Biolegend, 801201), as described by Toriyama et al[25]. We used
399 secondary antibodies conjugated with Alexa Fluor 488 (Invitrogen, A11008) or Alexa Fluor 594
400 (Invitrogen A11032), and observed with a confocal laser scanning microscope (LSM 710). The
401 lengths of all axons of 50 cells were measured for each coverage.
402
403 ***Traction force microscopy***
404 Traction force microscopy was performed as described in literatures[12,25]. Briefly, neurons
405 were cultured on polyacrylamide gels with embedded fluorescent microspheres (200 nm diameter;
406 Invitrogen). Time-lapse imaging of florescent microsphere and growth cones was performed at
407 37℃ using the confocal microscope (LSM710; Carl Zeiss) with a C-Apochromat 63x/1.2 W Corr
408 objective (Carl Zeiss). In the neuron, EGFP is expressed to track the growth. The growth cone was
409 monitored by the EGEP fluorescence and DIC images. The surface of polyacrylamide gels was
410 coated with laminin using the same procedure as that used to coat glass-bottom dishes (see
411 above).
412 Traction forces under the growth cones were detected by displacement of the beads from
413 their original positions. Force vectors were estimated from the displacement. To compare the forces
414 under different laminin densities, the magnitude of the force vectors of individual beads under the
415 growth cones were statistically analyzed and expressed separately as means ± SEM. The
416 quantification of traction force was performed using MATLAB code TFM2021 and software[35].
417

418

419 ***Statistical analysis***

420 Graphs were generated and statistical analyses were performed by using Microsoft Excel
421 and R. For nonparametric datasets, we used Mann–Whitney test to compare two groups, and
422 Kruskal–Wallis test with Dunn's multiple comparison to compare more than two groups.

423

424 **Acknowledgments**

425 We thank Dr. Ryohei Yasukuni and Dr. Kazunori Okano (Nara Institute of Science and
426 Technology, Japan) for fruitful discussions.

427

428 **Funding**

429 This research was supported in part by AMED under grant number 21gm0810011h0005,
430 ACT-X under grant number JPMJAX191K, and the Foundation of Nara Institute of Science and
431 Technology.

432

433 **Author Contributions**

434 S.Y. and Y.H. designed the research. N.I. supervised the research and contributed to presentation
435 of the mechanism of axon outgrowth. S.Y. performed almost all experiments and data analysis.
436 K.B. prepared primary cultured neurons. S.Y. and Y.H. wrote the article.

437 **References**

438 1. A. L. Kolodkin, M. Tessier-Lavigne, Mechanisms and molecules of neuronal wiring: a
439 primer. Cold Spring Harb Perspect Biol 3 (2011).
440
441 2. L. A. Lowery, D. Van Vactor, The trip of the tip: understanding the growth cone machinery.
442 Nat Rev Mol Cell Biol 10, 332-343 (2009).
443
444 3. K. Franze, Integrating Chemistry and Mechanics: The Forces Driving Axon Growth. Annu
445 Rev Cell Dev Biol 36, 61-83 (2020).
446
447 4. D. M. Suter, P. Forscher, Substrate-cytoskeletal coupling as a mechanism for the
448 regulation of growth cone motility and guidance. J Neurobiol 44, 97-113 (2000).
449
450 5. N. A. Medeiros, D. T. Burnette, P. Forscher, Myosin II functions in actin-bundle turnover in
451 neuronal growth cones. Nat Cell Biol 8, 215-226 (2006).
452
453 6. C. E. Chan, D. J. Odde, Traction dynamics of filopodia on compliant substrates. Science
454 322, 1687-1691 (2008).
455
456 7. T. Shimada et al., Shootin1 interacts with actin retrograde flow and L1-CAM to promote
457 axon outgrowth. J Cell Biol 181, 817-829 (2008).
458
459 8. Y. Kubo et al., Shootin1-cortactin interaction mediates signal-force transduction for axon
460 outgrowth. J Cell Biol 210, 663-676 (2015).
461
462 9. K. Baba et al., Gradient-reading and mechano-effector machinery for netrin-1-induced
463 axon guidance. Elife 7 (2018).
464
465 10. H. Hall, S. Carbonetto, M. Schachner, L1/HNK-1 carbohydrate- and beta 1 integrin-
466 dependent neural cell adhesion to laminin-1. J Neurochem 68, 544-553 (1997).
467
468 11. T. Esch, V. Lemmon, G. Banker, Local presentation of substrate molecules directs axon
469 specification by cultured hippocampal neurons. Journal of Neuroscience 19, 6417-6426 (1999).
470

471 12. K. Abe et al., Grip and slip of L1-CAM on adhesive substrates direct growth cone
472 haptotaxis. Proceedings of the National Academy of Sciences of the United States of America 115,
473 2764-2769 (2018).
474
475 13. S. Gupton, C. Waterman-Storer, Spatiotemporal feedback between actomyosin and focal-
476 adhesion systems optimizes rapid cell migration. Cell 125, 1361-1374 (2006).
477
478 14. J. de Rooij, A. Kerstens, G. Danuser, M. Schwartz, C. Waterman-Storer, Integrin-
479 dependent actomyosin contraction regulates epithelial cell scattering. Journal of Cell Biology 171,
480 153-164 (2005).
481
482 15. M. Benoit, D. Gabriel, G. Gerisch, H. Gaub, Discrete interactions in cell adhesion measured
483 by single-molecule force spectroscopy. Nature Cell Biology 2, 313-317 (2000).
484
485 16. M. Krieg et al., Tensile forces govern germ-layer organization in zebrafish. Nature Cell
486 Biology 10, 429-U122 (2008).
487
488 17. J Zheng, R E Buxbaum, S R Heidemann, Measurements of growth cone adhesion to
489 culture surfaces by micromanipulation. Journal of Cell Biology 15, 2049-2060 (1994).
490
491 18. Y. Hosokawa, Applications of the femtosecond laser-induced impulse to cell research.
492 Japanese Journal of Applied Physics 58 (2019).
493
494 19. Y. Hosokawa, M. Hagiyama, T. Iino, Y. Murakami, A. Ito, Noncontact estimation of
495 intercellular breaking force using a femtosecond laser impulse quantified by atomic force
496 microscopy. Proceedings of the National Academy of Sciences of the United States of America
497 108, 1777-1782 (2011).
498
499 20. A. Vogel, V. Venugopalan, Mechanisms of pulsed laser ablation of biological tissues.
500 Chemical Reviews 103, 577-644 (2003).
501
502 21. A. Vogel, J. Noack, G. Huttman, G. Paltauf, Mechanisms of femtosecond laser
503 nanosurgery of cells and tissues. Applied Physics B-Lasers and Optics 81, 1015-1047 (2005).
504

~~21~~22.T. Iino, M. Hagiyama, T. Furuno, A. Ito, Y. Hosokawa, Time-Course Statistical Evaluation of Intercellular Adhesion Maturation by Femtosecond Laser Impulse. Biophysical Journal 111, 2255-2262 (2016).

~~22~~23. K. Oikawa et al., Physical interaction between peroxisomes and chloroplasts elucidated by in situ laser analysis. Nat Plants 1, 15035 (2015).

~~23~~24. S. Yamada, T. Iino, Y. Bessho, Y. Hosokawa, T. Matsui, Quantitative analysis of mechanical force required for cell extrusion in zebrafish embryonic epithelia. Biology Open 6, 1575-1580 (2017).

~~24~~25. M. Toriyama et al., Shootin1: a protein involved in the organization of an asymmetric signal for neuronal polarization. Journal of Cell Biology 175, 147-157 (2006).

26. RH. Nichol IV, KM. Hagen, DC. Lumbard, EW. Dent, TM. Gómez, Guidance of Axons by Local Coupling of Retrograde Flow to Point Contact Adhesions. Journal of Neuroscience 17, 2267-2282 (2016).

27. D. Koch, WJ. Rosoff, J. Jiang, HM. Geller, JS. Urbach, Strength in the Periphery: Growth Cone Biomechanics and Substrate Rigidity Response in Peripheral and Central Nervous System Neurons. Biophysical Journal 102, 452-460 (2012).

~~25~~28. S. Palecek, J. Loftus, M. Ginsberg, D. Lauffenburger, A. Horwitz, Integrin-ligand binding properties govern cell migration speed through cell-substratum adhesiveness. Nature 385, 537-540 (1997).

~~26~~29. DiMilla PA, Barbee K, Lauffenburger DA. Mathematical model for the effects of adhesion and mechanics on cell migration speed. Biophysical Journal 60, 15-37 (1991).

~~27~~30. A. Huttenlocher, M. H. Ginsberg, A. F. Horwitz, Modulation of cell migration by integrin-mediated cytoskeletal linkages and ligand-binding affinity. Journal of Cell Biology 134, 1551-1562 (1996).

31. JC. Schense, JA. Hubbell, Three-dimensional Migration of Neurites Is Mediated by Adhesion Site Density and Affinity. Journal of Biological Chemistry 275, 6813-6818 (2000)

~~28~~32. M. P. Sheetz, D. P. Felsenfeld, C. G. Galbraith, Cell migration: regulation of force on extracellular-matrix-integrin complexes. Trends Cell Biol 8, 51-54 (1998).

~~29~~33. T. Minegishi, N. Inagaki, Forces to Drive Neuronal Migration Steps. Front Cell Dev Biol 8, 863 (2020).

~~30~~34. K. Hennig et al., Stick-slip dynamics of cell adhesion triggers spontaneous symmetry breaking and directional migration of mesenchymal cells on one-dimensional lines. Sci Adv 6, eaau5670 (2020).

35. T. Minegishi, R. Fujikawa, RF. Kastian, Y. Sakumura, N. Inagaki, Analyses of Actin Dynamics, Clutch Coupling and Traction Force for Growth Cone Advance. Journal of visualized experiments : JoVE 176 (2021).

555

556 **Figures**

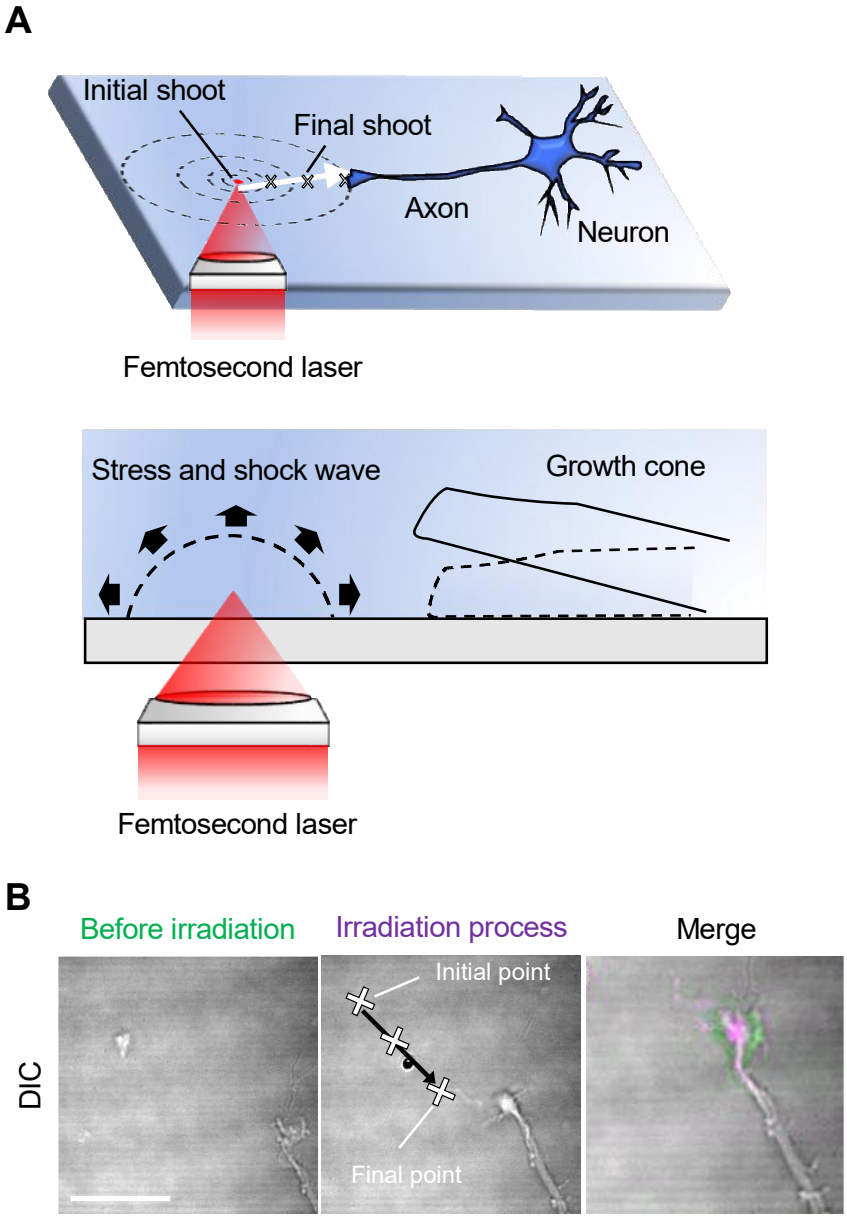

557

558 **Figure 1. Observation of adhesion breaking of an axonal growth cone by femtosecond laser-**
559 **induced impulsive force.** (A) Schematics of the spatial relation between the femtosecond laser
560 pulse and targeted axonal growth cone of a neuron on a glass substrate. The laser focal point was
561 sequentially moved closer to the growth cone, as indicated by an arrow in the upper cartoon. The
562 effect of the impulsive force to the growth cone was indicated in the lower cartoon, which is enlarged
563 view of the tip of the axon in the upper cartoon. (B) A representative result of adhesion breaking of
564 a growth cone observed by a differential interference contrast (DIC) imaging. The left panel is DIC

image before the laser irradiation at the final point. The middle panel indicates the laser irradiation process, in which the laser focal point (cross marks) was sequentially moved along an arrow in the image. The right panel is a merged images of the growth cones before and after the final laser irradiation, which are colorized in green and magenta, respectively. Cross marks are laser focal points. Scale bar, 10 μm.

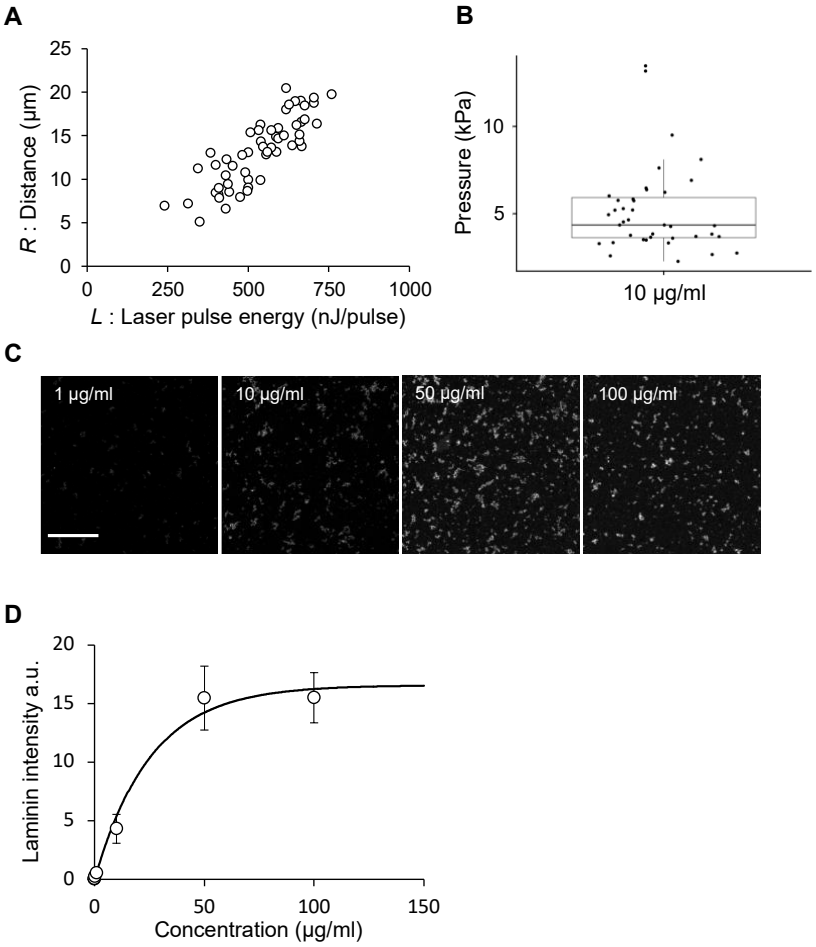

Figure 2. Quantitative evaluation of breaking force for growth cone adhesion by using femtosecond laser impulsive force. (A) Pulse energy *L* dependence of threshold distance *R* to break the growth cone adhesion on a glass substrate coated with a 10 μg/ml laminin solution, corresponding to an *A* of 0.45 (see Eq. [4]). *n* = 36. (B) Box-and-whisker plot of adhesion breaking threshold. Dots in the graph is the threshold calculated independently by substituting data from panel A into Eq. [2]. The mean value and standard deviation are 4.35 and 1.08 kPa, respectively. (C) Images of fluorescent dye-conjugated laminin on the substrate. Concentrations of the laminin solution used for the coating are indicated at the top. Scale bar, 10 μm. (D) Fluorescence intensity as a function of the laminin concentration. The fluorescence intensities were measured on substrates coated with laminin solutions with concentrations of 0.01, 0.1, 1, 10, 50, and 100 μg/ml. The fitting curve was calculated by Eq. [3], where I_{max} = 25.5 and *k* = 16.6. *n* = 50 for each concentration. Data are means ± SDs from three independent experiments.

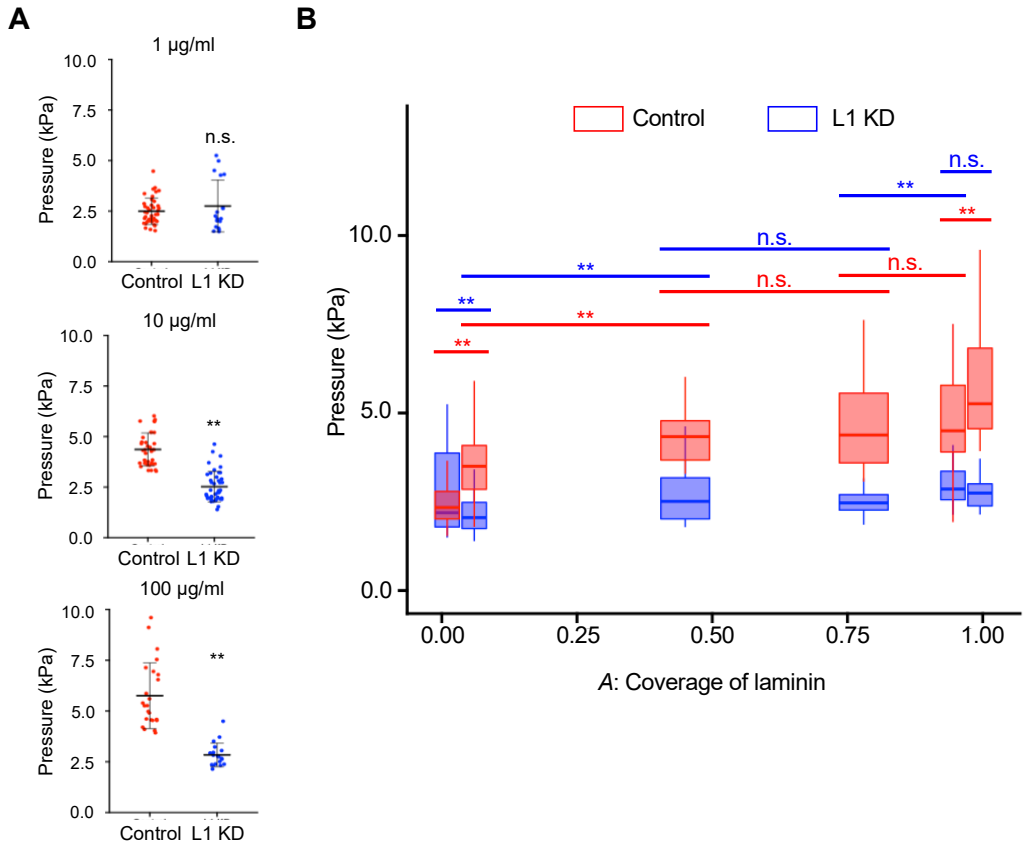

Figure 3. Adhesion breaking of growth cone on a laminin-coated substrate.

(A) Means and SDs of the adhesion breaking threshold. Dots in the graph is the threshold calculated independently by substituting data from panel A into Eq. [2]. The laminin concentration is indicated at the top. Red and blue dots indicate control neurons and L1CAM knockdown neurons, respectively. (B) Box-and-whisker plots of adhesion breaking threshold. Control neurons: n = 41, 35, 36, 12, and 25 signals for A = 0.01, 0.06, 0.45, 0.78, and 0.99, respectively. L1CAM knockdown neurons: n = 18, 44, 34, 20, and 19 signals for A = 0.01, 0.06, 0.45, 0.78, and 0.99, respectively. **p < 0.01 (two-tailed Student's t test), n.s., not significant.

598

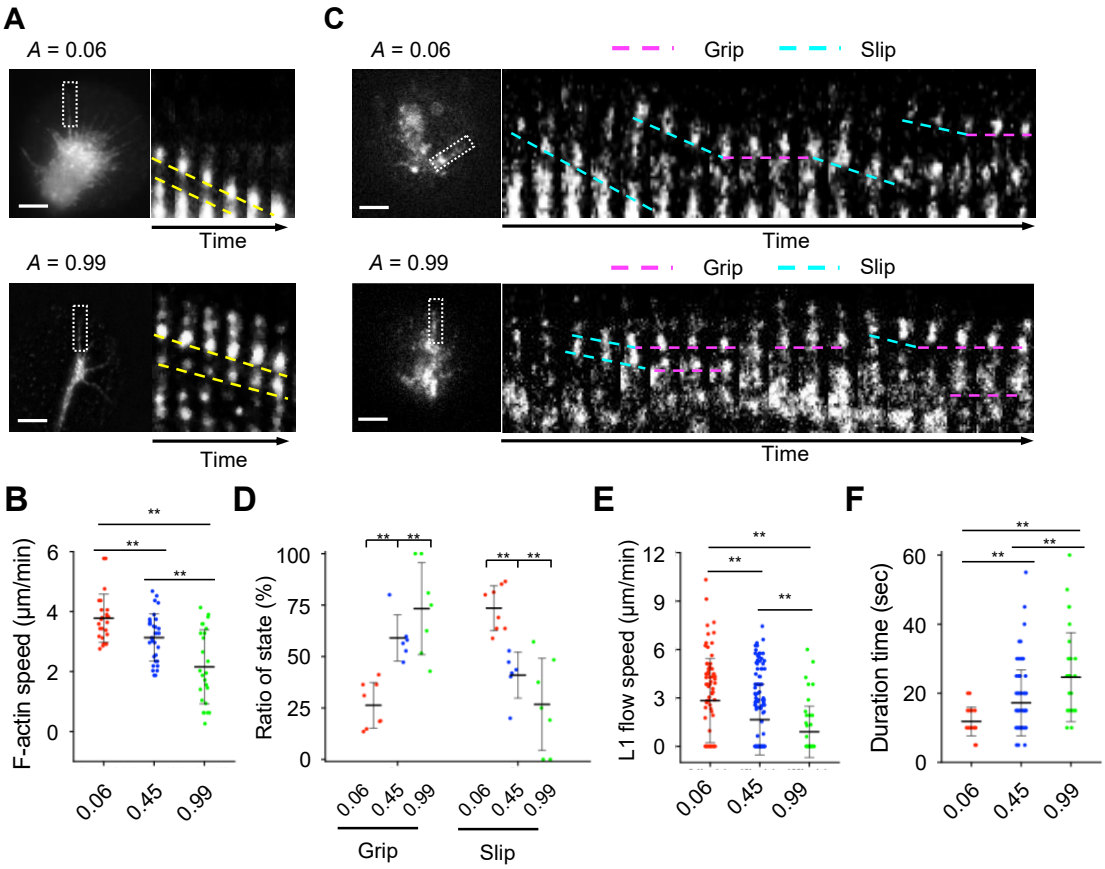

599

600

601 **Figure 4. Molecular dynamics of F-actin and L1CAM in the axonal growth cone detected by**
602 **fluorescence speckle microscopy.** (A) Fluorescence speckle images of the HaloTag-actin in a
603 filopodium extended from an axonal growth cone. The coverage of laminin (*A*) is indicated at the
604 top. Kymographs (right) depict HaloTag-actin behavior in boxed region in the image on the left.
605 Slope of the yellow dashed line corresponds to retrograde flow speed of the F-actin. Time interval
606 between frames, 5 s. Scale bar, 5 μm. (B) Retrograde flow speed of F-actin. n = 125, 160, and
607 130 signals for A = 0.06, 0.45, and 0.99, respectively. (C) Fluorescence speckle images of
608 L1CAM-HaloTag in a filopodium. Kymographs (right) depict L1CAM-HaloTag behavior in a boxed
609 region in the image on the left. Dashed pink and blue lines connect L1CAM in grip and slip states,
610 respectively. Time interval between frames, 5 s. Scale bar, 5 μm. (D) Ratios of the grip and slip
611 states of L1CAM-HaloTag in filopodia obtained from the kymograph analyses. n = 261, 450, and
612 197 signals for A = 0.06, 0.45, and 0.99, respectively. (E) Flow speed of L1CAM-HaloTag in the
613 slip state. The speed corresponds to slopes of dashed blue lines in panel C. (F) Duration time of
614 L1-HaloTag grip. White, red, and blue bars represent data for A = 0.06, 0.45, and 0.99,
615 respectively. Data are means ± SDs; $^{**}p < 0.01$.

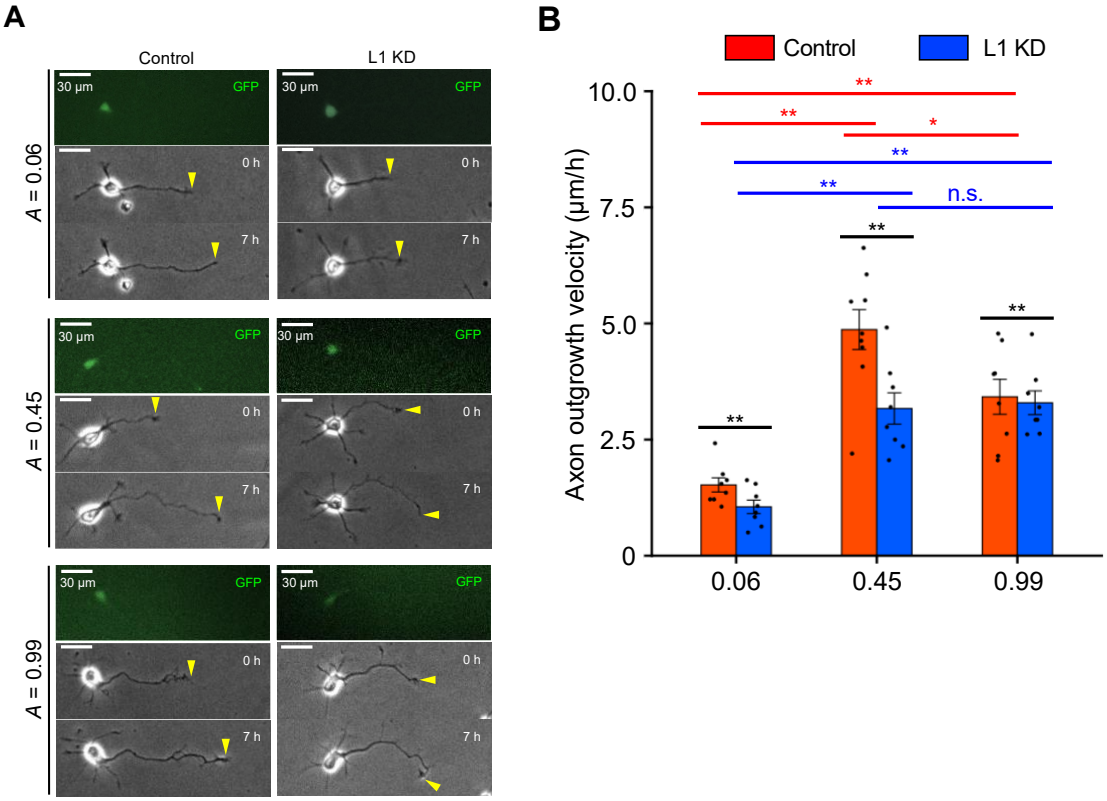

Figure 5. Growth cone migration on laminin-coated substrate.

(A) Time-lapse phase-contrast/fluorescence images of hippocampal neurons in control conditions (left panels) or L1 KD conditions (Right panels). Yellow arrowheads indicate growth cone at the first and last time-points, respectively. See also Video – and -. Scale bar: 30 µm. (B) Quantification of axon outgrowth velocity expressing control RNA (red) and L1-CAM miRNA (blue) for A = 0.06, 0.45, and 0.99, respectively. Control: n = 8, 9, and 8 for A = 0.06, 0.45, 0.78, and 0.99, respectively; L1 KD: n = 8, 8, and 8for A = 0.06, 0.45, and 0.99, respectively. Data are means ± SDs. Kruskal-Walls test. *$p < 0.05$, **$p < 0.01$. n.s., not significant.

627

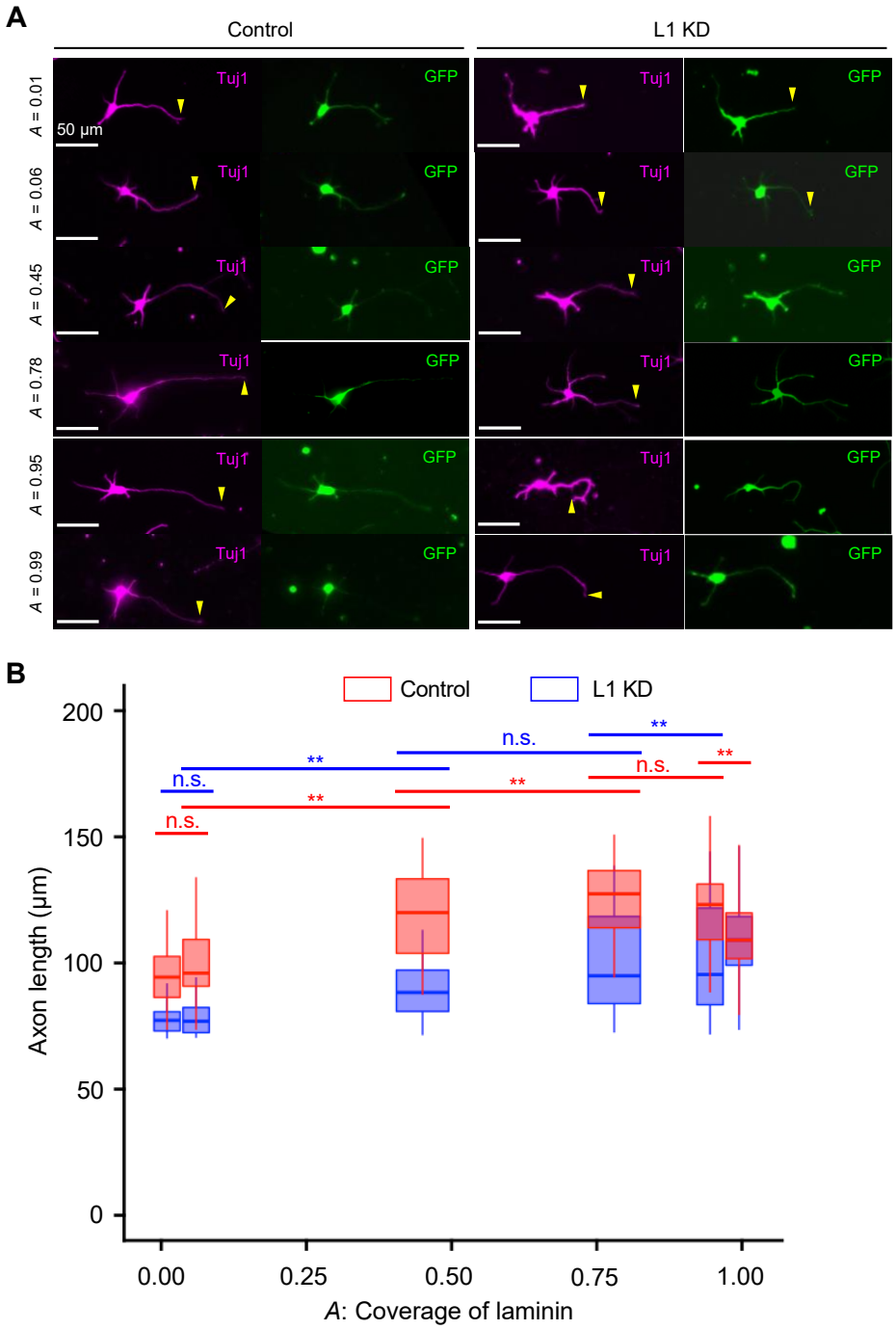
A
Control
L1 KD
A = 0.01
A = 0.06
A = 0.45
A = 0.78
A = 0.95
A = 0.99
Tuj1
GFP
50 µm
B
Control
L1 KD
Axon length (µm)
200
150
100
50
0
n.s.
**
0.00
0.25
0.50
0.75
1.00
A: Coverage of laminin

628

629

630

631 **Figure 6**. **Axon elongation on laminin-coated substrate.**

632 (A) Confocal images of neurons visualized with a GFP (green) and Tuj1 (Tubulin β3, magenta)
633 antibody. Neurons were cultured on polyacrylamide gels coated with laminin. The coverage of
634 laminin (*A*) is indicated on the left. Scale bar; 50 μm. (B) Box-and-whisker plots of axon length.
635 Control neurons (red): n = 91, 28, 79, 60, and 71 signals for A = 0.01, 0.06, 0.45, 0.78, and 0.99,
636 respectively; L1CAM knockdown neurons (blue): n = 43, 49, 73, 103, and 48 signals for A = 0.01,
637 0.06, 0.45, 0.78, and 0.99, respectively. Kruskal-Walls test. *p < 0.05, **p < 0.01. n.s., not
638 significant.

639

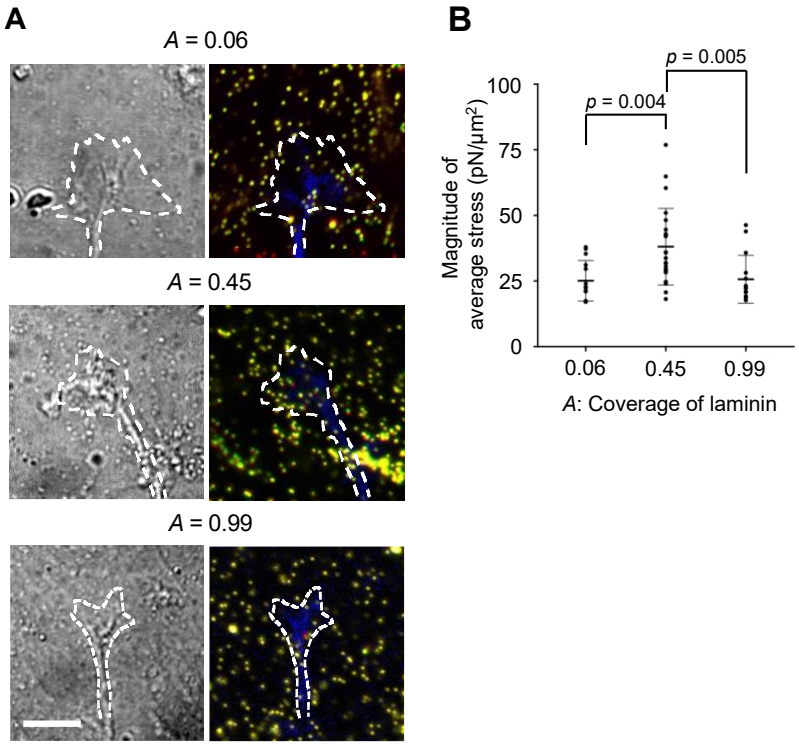

640

641 **Figure 7. Measurement of traction force on a laminin-coated substrate.**

642 (A) DIC (left panels) and fluorescence images (right panels) of an axonal growth cone cultured on
643 polyacrylamide gels with embedded 200 nm fluorescent beads. Dashed lines indicate the boundary
644 of the growth cone. The blue color in the dashed line is due to EGFP which is expressed in the
645 neuron to track the growth cone position. The original and displaced bead positions in the gel are
646 indicated by green and red colors in fluorescence images, respectively. The yellow color overlaps
647 the green and red colors, i.e. the bead is rarely displaced. Laminin coverage *A* is shown at the top
648 of the panel column. Scale bar; 10 μm. (B) Magnitude of the traction forces under axonal growth
649 cones. Data represent mean ± SEM (error bars).

650